Tunable terahertz fishnet metamaterial

Chang, Cheng-Ling; Wang, Wei-Chih; Lin, Hong-Ren; Ju Hsieh, Feng; Pun, Yue-Bun; Chan, Chi-Hou

Published in:
Applied Physics Letters

Published: 15/04/2013

Document Version:
Final Published version, also known as Publisher's PDF, Publisher's Final version or Version of Record

Published version (DOI):
10.1063/1.4801648

Publication details:
Chang, C.-L., Wang, W.-C., Lin, H.-R., Ju Hsieh, F., Pun, Y.-B., & Chan, C.-H. (2013). Tunable terahertz fishnet metamaterial. *Applied Physics Letters*, *102*(15), Article 151903. https://doi.org/10.1063/1.4801648

Applied Physics Letters

Tunable terahertz fishnet metamaterial

Cite as: Appl. Phys. Lett. **102**, 151903 (2013); https://doi.org/10.1063/1.4801648
Submitted: 20 September 2012 • Accepted: 28 March 2013 • Published Online: 15 April 2013

Cheng-Ling Chang, Wei-Chih Wang, Hong-Ren Lin, et al.

Tunable terahertz fishnet metamaterial

Cheng-Ling Chang,[1] Wei-Chih Wang,[1,2,3] Hong-Ren Lin,[1] Feng Ju Hsieh,[1] Yue-Bun Pun,[4] and Chi-Hou Chan[4]
[1]*Department of Mechanical Engineering, University of Washington, Seattle 98195, Washington, USA*
[2]*Department of Electrical Engineering, University of Washington, Seattle 98195, Washington, USA*
[3]*Medical Device Innovation Center, National Cheng Kung University, Tainan, Taiwan*
[4]*Department of Electrical Engineering, City University of Hong Kong, Hong Kong, China*

(Received 20 September 2012; accepted 28 March 2013; published online 15 April 2013)

This paper describes and demonstrates a terahertz (THz) frequency tunable fishnet metamaterial (TFMM) using an electrically controlled polymer dispersed liquid crystal (PDLC) matrix. In contrast to other PDLC-based devices, the TFMM employs a novel method for encapsulating PDLC using a thin (1.5 μm) polyimide "skin layer" to form a uniform surface for metal electrodes while minimizing the Fabry-Perot effect of the skin layer on the TFMM measurements. The tunability was verified by measuring the frequency shift in the reflection coefficient (0.01 THz), with an observed minimum negative refractive index of −15 at 0.55 THz. © *2013 AIP Publishing LLC* [http://dx.doi.org/10.1063/1.4801648]

Metamaterials are artificial materials designed to produce exotic effects, such as negative refractive indices, enabling the design of unusual but potentially useful technologies prominently known as super lenses[1] and invisibility cloaks.[2] However, due to the challenges of realizing an isotropic, low-loss, and broadband metamaterial for its original purposes, the focus of the later metamaterials studies shifts towards achieving tunable, nonlinear, and sensing functionalities.[3] Amongst these emerging applications, devices using tunable metamaterials have drawn the most attention.[4] This is because tunable metamaterials have unique, powerful applications, such as active filters,[4–6] tunable perfect obsorber,[7] electro-optical switch,[8,9] variable refractive index materials,[10,11] highly directional high gain antennas,[12] and wide-angle beam steering devices.[13]

There are several methods of tuning metamaterials such as geometry alteration,[14] Schottky diodes,[4] and electro-optic (EO) tuning.[10,11,15,16] EO tuning is the most commonly used method, because it is voltage controlled and provides a large tuning range. Among EO materials, liquid crystal (LC) has received a great deal of study due to its broad range of operating frequencies, large dielectric change,[5,11,15,17] and the effect on the nonlinear properties of metamaterials.[17] However, LC devices require a confined chamber for LC (e.g., a LC cell). The addition of a LC cell into a design not only increases the fabrication difficulty but also affects the subsequent material characterization process.[10,15,18]

Polymer dispersed liquid crystal (PDLC) is a hybrid material that combines the mechanical strength of a solid polymer with the EO characteristics of LC.[19] The porous cellular structure of the polymer provides numerous small pockets to contain LC droplets, allowing the LC molecules to freely rotate inside the pores under the influence of an external voltage field. Thus, for most tunable EO metamaterial designs, using PDLC removes the unwanted LC cell effects and simplifies the fabrication process.

In this paper, a novel tunable fishnet metamaterial infiltrated with the PDLC-TFMM and an ultra-thin polyimide (1.5 μm) "skin layer" is experimentally demonstrated. Many tunable PDLC devices, such as phase shifters[20] or tunable capacitors[21] routinely use a thick cover layer (at least 1 mm thick) to seal the volatile LC inside the porous polymer matrix. The absorption and multiple internal reflections (Fabry-Perot effect) from this layer can affect the overall light transmission (S21) and reflection (S11),[22] which are the essential in determining the overall performance of a metamaterial.[23] Therefore, using solution-processable polyimide to create a micron range skin layer can reduce the absorption loss and Fabry-Perot effect, directly benefiting the device performance and ease of characterization.

Our PDLC-TFMM device (Figure 1(a)) is designed to operate in the terahertz (THz) range. The fishnet unit cell (with dimensions of $L = 150$ μm) is symmetric, which makes the operation of the PDLC-TFMM independent of the incident light polarization in xy plane[14] (Figure 1(a)). The PDLC ($p = 10$ μm) and polyimide (PI) skin layer ($m = 1.5$ μm) are sandwiched between the two gold fishnet electrodes ($a = 250$ nm) as shown in Figure 1(b). The entire structure is fabricated on a double side polished silicon (DSP-Si) wafer with thickness $s = 1$ mm and resistivity $> 10\,000\,\Omega$ cm. The high resistivity of the thick DSP-Si is desirable for isolating higher-order internal reflection modes and reducing transmission loss, which assists in removing the substrate effect and enhances the transmission properties of the entire device. A chromium (Cr) adhesion layer ($c = 5$ nm) holds the gold to the DSP-Si. Figure 2(a) shows that the PI skin layer can successfully prevent the LC from escaping the PDLC. When the PI skin layer is removed from the center of the device also shown in the figure, the exposed LC molecules will escape and form droplets on top of the PDLC. Figure 2(b) illustrates how the unsealed LC escapes the porous polymer matrix. In addition to sealing the PDLC, the thermally stable and mechanically flexible PI[24] also protects the PDLC from being damaged during metal deposition, making it possible to directly pattern the metal layer (e.g., metal sputtering[14,25]) onto the PDLC. It is possible small amount of LC can still escape from the side of the unprotected PDLC. However, the leakage should be

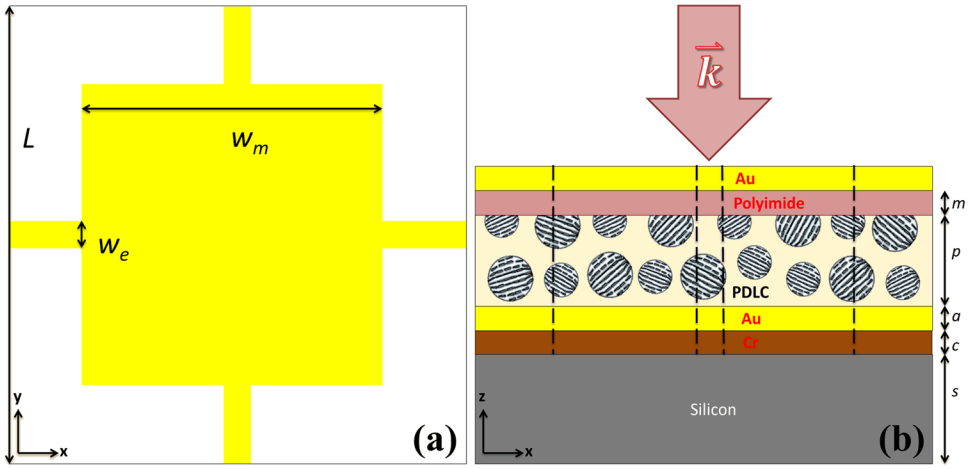

FIG. 1. PDLC-TFMM unit cell: (a) overhead view of unit cell with $L = 150\ \mu$m, $w_m = 115\ \mu$m, and $w_e = 10\ \mu$m; (b) cross section of the unit cell, with thicknesses of $m = 1.5\ \mu$m, $p = 10\ \mu$m, $a = 0.25\ \mu$m, $c = 5$ nm, and $s = 1$ mm.

minimum and should not affect the final measurement because the area of the device (12×12 mm^2) is much greater than its thickness (10 μm). Furthermore, the actual PI/PDLC area is made much larger than the fishnet device area. The final PDLC-TFMM device (Figure 3(a)) possesses two major test areas for the THz radiation to probe: (1) the fishnet area and (2) the DSP-Si area for the reference field measurement. The completed fishnet unit cells are arranged in a periodic 80 by 80 cell matrix in the x-y directions. The copper tape and silver epoxy connect the upper and lower fishnet electrodes to the power supply, providing the biasing voltage for the PDLC.

The PDLC used in the study is a UV-curable acrylate-based pre-polymer mixed with 4-pentyl-4′-cyano-biphenyl (5BC) LC (45 wt. %). The UV curing process is performed using a 100 mW LED light (spectral range of 350 to 400 nm) with a 3000 mJ exposure dose.[19] The resulting droplet size is measured in the tenths and hundredths of nanometers. So far, there is no direct method for observing the on and off states of PDLC between the gold-covered fishnet electrodes. Instead, the state is determined by observing the opacity of the PDLC through the electric field fringe effect around the edges of the electrodes. As shown in Figure 3(c)), a significant fringe effect around electrodes is observed at a 280 V bias, which makes the completely opaque, dark-looking PDLC on the edges (Figure 3(b)) more transparent around the fishnet edges (Figure 3(c)). At 280V bias, we assume the field strength is sufficient to turn on the PDLC.

The PDLC-TFMM is characterized by a terahertz time domain spectroscope (THz-TDS) from EKSPLA (Vilnius, Lithuania) based on the photoconductive THz generation and detection technique.[26] The emitted THz radiation from EKSPLA is focused on the fishnet (12×12 mm total area) with normal incidence and a 4 mm beam size. The probed area is shown in the red-dashed square in Figure 3(a). The sample (fishnet) and reference fields are first converted from time domain (Figure 4) to frequency domain by Fast Fourier Transform (FFT). Then, the transmission (S21) and reflection (S11) are obtained by normalizing the sample fields to

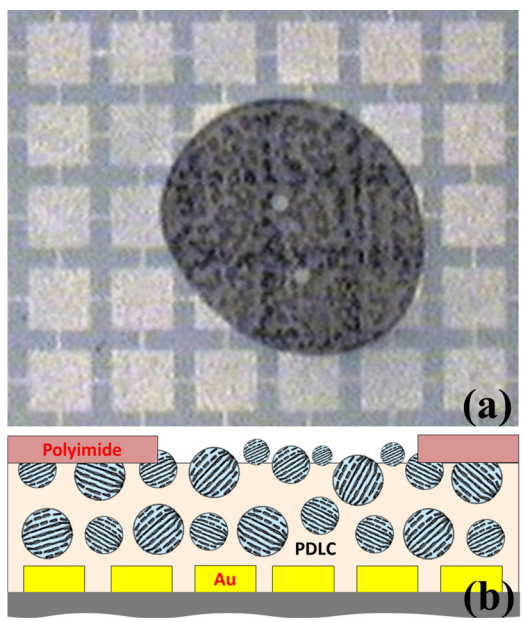

FIG. 2. PDLC with and without polyimide skin layer: (a) overhead view of the liquid crystal droplets accumulating at center of the device where skin layer is removed; (b) cross section of the PDLC fabricated on top of the fishnet pattern and silicon substrate.

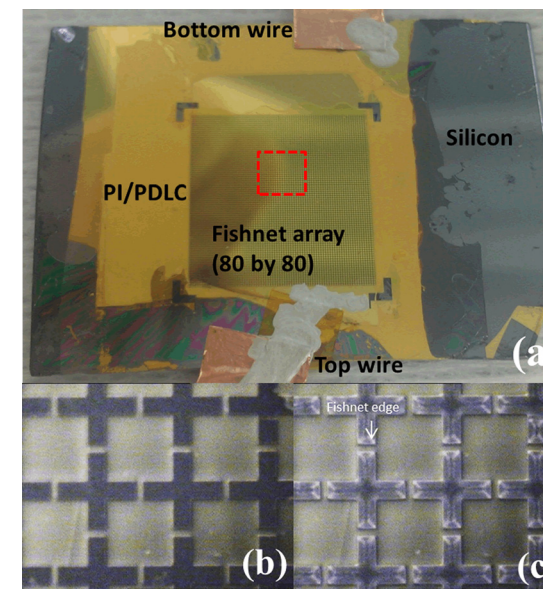

FIG. 3. PDLC-TFMM testing sample: (a) perspective view of testing sample; (b) microscopic view of PLDC-TFMM at 0 V; (c) microscopic view of PLDC-TFMM at 280 V.

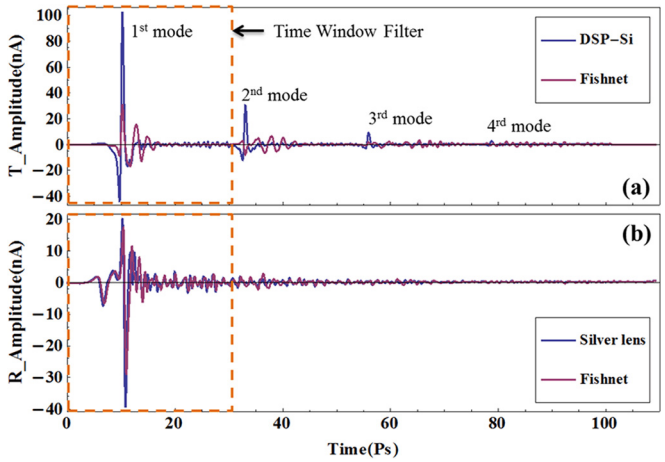

FIG. 4. Time domain signals of PDLC-TFMM at 0 V bias: (a) transmission measurement with time window applied to remove multiple internal reflections from DSP-Si; (b) reflection measurement with time window applied. Higher FP modes decay faster compared to transmission mode.

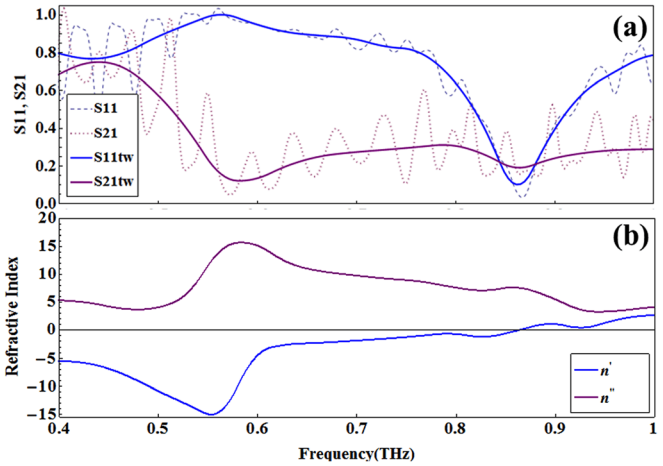

FIG. 5. (a) S11 and S21 of PDLC-TFMM at 0 V bias before and after time window is applied. The dashed and dotted lines represent original S11 and S21. Significant FP effect is observed in original S21. Solid lines are S11 (S11tw) and S21 (S21tw) with time window applied. (b) Real and imaginary refractive index of PDLC-TFMM at 0 V bias is calculated based on S11tw and S21tw.

the reference fields. The reference field of S21 is from the field transmitted through the DSP-Si substrate while the reference field of S11 is reflected from silver lens. In the S11 measurement, the probed surfaces of the sample and the silver lens are located in the same plane to avoid phase differences.

In the transmission measurement (Figure 4(a)), the Fabry Perot (FP) effect from the DSP-Si substrate[22] can be clearly seen and separated in time domain because of the DSP-Si thickness. This can help isolate the substrate effect from the PDLC-TFMM/DSP-Si composite when a time window (the dashed orange box) is applied to remove the higher modes. However, the time window technique can remove data points from the measurements, resulting in reduced accuracy. In the reflection measurement, we can see the direct benefit of the skin layer in minimizing the FP effect (Figure 4(b)). The FP effect from the ultra-thin skin layer is very small compared to the PDLC-TFMM. The remaining FP effect comes from the DSP-Si. However, the higher FP modes from the DSP-Si decay much faster in the reflection measurement than the higher modes in the transmission measurement.

To understand the negative refractive index effect of the PDLC-TFMM, we measure the S21 and S11 with zero bias and apply the time window technique (Figure 5). Then, following well-established methods,[23,27] the refractive index (Figure 5(b)) can be calculated from the S11 and S21 using

$$n\,k\,L_z = \pm\cos^{-1}\frac{1 - S11^2 + S21^2}{2\,S21} + 2\,\pi\,m,$$

where n is the effective refractive index, k is the incident wave number, L_z $(12.005\,\mu\text{m})$ is the unit cell size in the wave propagating direction, and m is the branch index. The ambiguous m and $\pm$ sign of arccosine function can be solved by assuming the PDLC-TFMM is lossy and passive. In our case, m is equal to zero. The reference planes for measuring S11 and S21 are located at the physical boundaries of the PDLC-TFMM. We first compare the S21 and S11 of the PDLC-TFMM (Figure 5(a)) to previous simulation results[14,18] where the dimensions of the fishnet patterns are exactly the same. From our experiment results, we observe that the S21 dip occurs at a much lower frequency (0.58 THz) than the frequency of the S11 dip (0.87 THz), while in the simulation the frequencies of the S11 and S21 dips are close to each other. The misalignment between top and bottom fishnet layers, the effect of extra PI skin layer, and material loss from PDLC and DSP-Si might be the reasons why S21 occurs at such low frequency and S21 pass band (0.6–0.86 THz) is suppressed.[18] The frequency of S21 dip also affects where the minimum value of the real refractive index (n′) occurs. From our calculation minimum n′ occurs at 0.55 THz with a value of −15 (Figure 5(b)). We observe that n′ are all negative from 0.4 to 0.86 THz and become positive after operation frequency passes 0.86 THz. Also, the imaginary refractive indexes (n″) are all positive from 0.4 to 1 THz which satisfies the assumption that the PDLC-TFMM is lossy.

The tuning effect of the PDLC-TFMM is shown by measuring S11 (Figure 6(a)) at 0 V and 280 V with the time window technique applied. When the 280 V bias is applied, the frequency of the S11 dip shifts downward from 0.87 to 0.86 THz, giving a total frequency shift of 10 GHz. The decreased resonant frequency of S11 dip can be explained by the increased dielectric property of the 5BC molecules inside the PDLC when they are forced to align to external field. This increases the capacitance between the fishnet electrodes, resulting in a reduced magnetic resonant frequency (a function of $\frac{1}{\sqrt{Capacitance}}$ (Ref. 18)). Note that from previous experimental results,[17] the dielectric constant change of 5BC from the ordinary state ($\varepsilon_o = 2.403$) to the extraordinary state ($\varepsilon_e = 2.723$) is 0.32 at 1 THz. However, the dielectric constant change of the PDLC in our device is less than the optimal (e.g., 100 wt. %) value, as the 5BC in PDLC is only 45 wt. % and is not pre-aligned in the PDLC.[28] A larger resonant frequency shift of S11 can be expected if a higher LC wt. % ratio is used and pre-aligned within the PDLC. Furthermore, in our experiment, significant positive and negative phase shifts of S11 are observed, with a 70° positive phase shift and a 10 GHz frequency shift achieved near 0.86 THz at 280 V (Figure 6(b)). Away from the resonant region,

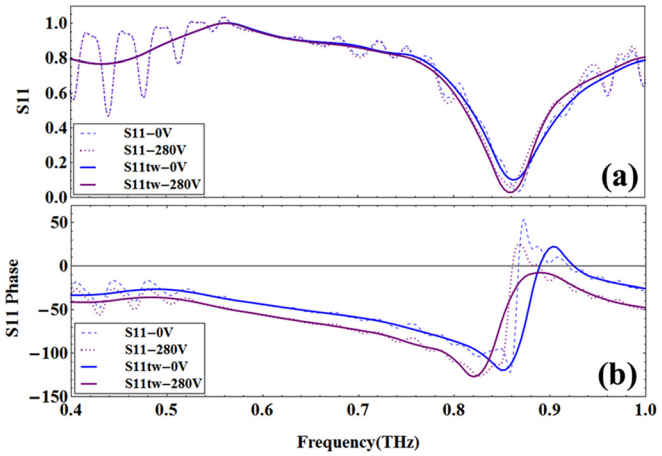

FIG. 6. Tunability of PDLC-TFMM at 0 V and 280 V bias can be seen in (a) S11 and (b) S11 phase. The dashed and dotted lines represent original S11 at 0 V and 280 V. Significant FP effect can be seen in the lower frequency range (0.4 to 0.55 THz) but the effect can be removed by time window technique.

the phase shift becomes negative which is similar to the results shown by the metamaterial phase shifter.[29]

So far, the tuning effects of the S21 of the PDLC-TFMM cannot be observed because the current PDLC-TFMM design causes dielectric breakdown to occur easily around the "net" part of the fishnet, and a reduction in the tuning range of the PDLC-TFMM was discovered that prevents consistent measurements of dielectric change of the PDLC. However, as the tuning effect of S11 also affects S21, the concept of a tunable refractive index from our PDLC-TFMM has been shown.

In conclusion, we have fabricated a novel PDLC-TFMM incorporating an ultra-thin PI skin layer in the design, improving the ease of fabrication and S11 measurements. We have demonstrated the tunability of the PDLC-TFMM by observing the S11 resonant frequency and phase shift 10 GHz and 70° at 280 V, respectively. We also calculated the effective refractive index of the PDLC-TFMM, which can achieve a minimum of −15 at 0.55 THz.

We acknowledge the support by State Key Laboratory of Millimeter Waves at the City University of Hong Kong and Micro technology Laboratory at University of Washington. We thank Dr. Xiao Gan for the help on the device characterization and Kwok-On Tsang, Alvin Tsai, Xiao Lin, and Fei Xiu for the device fabrication.

[1]J. B. Pendry, Phys. Rev. Lett. **85**, 3966 (2000).
[2]D. Schurig, J. J. Mock, B. J. Justice, S. A. Cummer, J. B. Pendry, A. F. Starr, and D. R. Smith, Science **314**(5801), 977 (2006).
[3]N. I. Zheludev and Y. S. Kivshar, Nature Mater. **11**(11), 917 (2012).
[4]H.-T. Chen, W. J. Padilla, J. M. O. Zide, A. C. Gossard, A. J. Taylor, and R. D. Averitt, Nature **444**(7119), 597 (2006).
[5]W. Hu, R. Dickie, R. Cahill, H. Gamble, Y. Ismail, V. Fusco, D. Linton, N. Grant, and S. Rea, IEEE Microw. Wirel. Compon. Lett. **17**(9), 667–669 (2007).
[6]X. Deng, N. Liu, and L. An, Chin. Sci. Bull. **54**(12), 2002 (2009).
[7]D. Shrekenhamer, W.-C. Chen, and W. J. Padilla, e-print arXiv:1206.4214.
[8]O. Buchnev, J. Y. Ou, M. Kaczmarek, N. I. Zheludev, and V. A. Fedotov, Opt. Express **21**(2), 1633 (2013).
[9]M. Decker, C. Kremers, A. Minovich, I. Staude, A. E. Miroshnichenko, D. Chigrin, D. N. Neshev, C. Jagadish, and Y. S. Kivshar, Opt. Express **21**(7), 8879–8885 (2013).
[10]J. A. Bossard, L. Xiaotao, L. Ling, Y. Seokho, D. H. Werner, B. Weiner, T. S. Mayer, P. F. Cristman, A. Diaz, and I. C. Khoo, IEEE Trans. Antennas Propag. **56**(5), 1308 (2008).
[11]A. Minovich, D. N. Neshev, D. A. Powell, I. V. Shadrivov, and Y. S. Kivshar, Appl. Phys. Lett. **96**(19), 193103 (2010).
[12]C. Caloz and T. Itob, *Electromagnetic Metamaterials: Transmission Line Theory and Microwave Applications* (Wiley-Interscience, 2006).
[13]J. Valentine, S. Zhang, T. Zentgraf, E. Ulin-Avila, D. A. Genov, G. Bartal, and X. Zhang, Nature **455**(7211), 376 (2008).
[14]P. Ding, E. J. Liang, W. Q. Hu, L. Zhang, Q. Zhou, and Q. Z. Xue, Photonics Nanostruct. Fundam. Appl. **7**(2), 92 (2009).
[15]F. Zhang, Q. Zhao, W. Zhang, J. Sun, J. Zhou, and D. Lippens, Appl. Phys. Lett. **97**(13), 134103 (2010).
[16]Z. L. Samson, K. F. MacDonald, F. De Angelis, B. Gholipour, K. Knight, C. C. Huang, E. Di Fabrizio, D. W. Hewak, and N. I. Zheludev, Appl. Phys. Lett. **96**(14), 143105 (2010).
[17]N. Vieweg, C. Jansen, M. Khaled Shakfa, M. Scheller, N. Krumbholz, R. Wilk, M. Mikulics, and M. Koch, Opt. Express **18**(6), 6097 (2010).
[18]F. Zhang, W. Zhang, Q. Zhao, J. Sun, K. Qiu, J. Zhou, and D. Lippens, Opt. Express **19**(2), 1563 (2011).
[19]Merck, Merck Specialty Chemicals, Ltd., Southampton, England, 2002.
[20]T. Kamei, N. Quoc Dinh, and Y. Utsumi, Mol. Cryst. Liq. Cryst. **476**(1), 15 (2007).
[21]W.-P. Shih, S.-Y. Chung, Y.-Y. Chen, W.-J. Wu, and P.-Z. Chang, IEEE Trans. Electron Devices **55**(10), 2568 (2008).
[22]T. D. Dorney, R. G. Baraniuk, and D. M. Mittleman, J. Opt. Soc. Am. A **18**(7), 1562 (2001).
[23]D. R. Smith, S. Schultz, P. Markoš, and C. M. Soukoulis, Phys. Rev. B **65**, 195104 (2002).
[24]M. Ree, K.-J. Chen, D. P. Kirby, N. Katzenellenbogen, and D. Grischkowsky, J. Appl. Phys. **72**(5), 2014 (1992).
[25]N. Liu, L. Fu, S. Kaiser, H. Schweizer, and H. Giessen, Adv. Mater. **20**(20), 3859 (2008).
[26]P. U. Jepsen, D. G. Cooke, and M. Koch, Laser Photonics Rev. **5**(1), 124 (2011).
[27]X. Chen, T. M. Grzegorczyk, B.-I. Wu, J. Pacheco, and J. Au Kong, Phys. Rev. E **70**, 016608 (2004).
[28]T. Kamei, N. Quoc Dinh, and Y. Utsumi, Mol. Cryst. Liq. Cryst. **476**(1), 15/[261] (2007).
[29]M. A. Y. Abdalla, P. Khoman, and G. V. Eleftheriades, presented at the 36th European Microwave Conference, Manchester, UK, 2006.